npj Computational Materials

www.nature.com/npjcompumats

ARTICLE OPEN

Check for updates

Anion charge and lattice volume dependent lithium ion migration in compounds with *fcc* anion sublattices

Zhenming Xu[1], Xin Chen[2], Ronghan Chen[1], Xin Li[3] and Hong Zhu[1]✉

Proper design principles are essential for the efficient development of superionic conductors. However, the existing design principles are mainly proposed from the perspective of crystal structures. In this work, the face-centered cubic (*fcc*) anion sublattices were creatively constructed to study the effects of anion charge and lattice volume on the stability of lithium ion occupation and lithium ion migration by the density functional theory calculations. Both the large negative anion charges and large lattice volumes would increase the relative stabilities of lithium-anion tetrahedron, making lithium ions prefer to occupy the tetrahedral sites. For a tetrahedral lithium ion migration to its adjacent tetrahedral site through an octahedral transition state, the smaller the negative anion charge is, the lower the lithium ion migration barrier will be. While for an octahedral lithium ion migration to its adjacent octahedral site through a tetrahedral transition state, the more negative anion charge is, the lower the lithium ion migration barrier will be. New design principles for developing and optimizing superionic conductors with the *fcc* anion sublattice were proposed. Low lithium ion migration barriers would be achieved by adjusting the non-lithium elements within the same crystal structure to obtain the desired electronegativity difference between the anion element and the non-lithium cation element.

npj Computational Materials (2020)6:47 ; https://doi.org/10.1038/s41524-020-0324-7

INTRODUCTION

Safety is the most important concern when using the commercial lithium ion batteries (LIBs) in the application scenarios of the large-scale energy storage, such as electric vehicles. Replacing the currently employed flammable liquid electrolytes in LIBs with the solid-state electrolyte (SSE) materials and collocating with the lithium metal anodes to construct the all-solid-state lithium ion batteries (ASSLIBs) not only could solve the battery safety issues, but also remarkably enhance the energy density of battery systems[1–3]. Correspondingly, the construction of practical ASSLIBs needs SSE materials to achieve lithium ion fast conduction with low activation energies (<300 meV) and high lithium ionic conductivities (10^{-3}–10^{-2} S cm^{-1}) at room temperature. So far, some superionic conductors, such as $Li_7La_3Zr_2O_{12}$[4], $Li_{1+x}Al_xTi_{2-x}(PO_4)_3$[5] oxides and $Li_{10}GeP_2S_{12}$[6], $Li_7P_3S_{11}$[7] sulfides have been widely studied as SSE materials, and the state-of-the-art ionic conductivities of 12–17 mS cm^{-1} at room temperature are experimentally realized in $Li_{10}GeP_2S_{12}$ and $Li_7P_3S_{11}$ sulfides.

To efficiently develop more advanced superionic conductors for ASSLIBs, the better understanding of fast ion migration mechanism in the state-of-the-art superionic conductors and the development of proper design principles are quite essential. Ceder et al.[8] have proposed an important design principle for superionic conductors that the body-centered cubic anion sublattice with face-sharing lithium-anion tetrahedra allows the low activation energy for lithium ion migration, which is successfully guiding the high-throughput screening of new superionic conductors[9]. Hautier et al. found the distorted lithium-sulfur polyhedra in $LiTi_2(PS_4)_3$ provide the smooth energy landscape combining small activation energy barriers with numerous migration paths, and proposed the design concept of "frustrated energy landscape" for superionic conductors[10]. As the crystallography and mineralogy literatures showing Li^+ and Zn^{2+} are most often found in four-coordination, Mg^{2+} in six-coordination, and Ca^{2+} in eight-coordination, the mobile species at their equilibrium sites with more unfavored coordination environments than their intermediate sites would be correlated with high ionic conductivities[11,12], e.g. Li^+ and Zn^{2+} in the olivine and layered structure have better diffusivity than the spinel, and similarly Mg^{2+} in spinel has superior diffusivity compared to the olivine and layered. However, the high-throughput screenings of fast lithium ion conductors by Xiao et al. show the activation energies of lithium ion migration in the olivine-structures are lower than those of the layered and even spinel structures[13].

In addition to the above understandings of lithium topology structure features, the interactions between mobile lithium species and crystal sublattice were also studied. It is generally accepted that the Columbic force dominates the interactions between the mobile cation and its adjacent anion sublattice in ionic materials[14–16]. In spinel $LiMn_2O_4$, the different valence states of Mn ions and their arrangements surrounding lithium ions have important effects on the activation energy barrier of lithium ion migrations[14]. Krauskopf et al.[17] found the lower electronegativity of Sn *vs*. Ge (1.7 *vs*. 2.0) lead to more electron density on S^{2-} atoms in $Li_{10}SnP_2S_{12}$, which in turn lead to the stronger Li^+-S^{2-} Coulombic attractions, thereby inhibiting lithium ion transport compared to $Li_{10}GeP_2S_{12}$. Our previous study of the chalcopyrite-structured $LiMS_2$ (*M* are transition metals, from Ti to Ni) materials with the same crystal structure demonstrates that the more negative anion charges resulted from the larger electronegativity difference between *M* and S elements would increase the activation energy barrier for lithium ion migration between the two adjacent tetrahedral (*Tet*) sites through an octahedral (*Oct*) transition state, namely *Tet-Oct-Tet* pathway[15]. In addition, Mo et al. constructed an artificial face-centered cubic (*fcc*) anion sublattice of the monovalent S^- in comparison with the bivalent

[1]University of Michigan–Shanghai Jiao Tong University Joint Institute, Shanghai Jiao Tong University, 800 Dongchuan Road, Shanghai 200240, China. [2]School of Materials Science and Engineering, Shanghai Jiao Tong University, 800 Dongchuan Road, Shanghai 200240, China. [3]Harvard John. A. Paulson School of Engineering and Applied Sciences, Harvard University, 29 Oxford Street, Cambridge, MA 02138, USA. ✉email: hong.zhu@sjtu.edu.cn

S^{2-} with a constant lattice volume, and found activation energy barrier for lithium ion migration along *Tet-Oct-Tet* pathway in the monovalent S^{-} sublattice is smaller than that of the bivalent S^{2-} sublattice[16]. According to these findings of the tetrahedral lithium ion migration, we have predicted a new lithium superionic conductor of Li_2CuPS_4 with the tetrahedral lithium occupations in an *fcc*-type anion sublattice and the relatively small electronegativity difference between the sulfur anion and copper cation[18]. On the contrary, in Li_3MI_6 (M = Sc, Y, and La) compounds with the octahedral lithium occupations, the more negative I anion charges would lower the activation energy barrier for lithium ion migration along *Oct-Tet-Oct* pathways[19]. Here comes the question, why anion charge shows the reverse influence on the activation energy barrier for lithium ion migration along the *Tet-Oct-Tet* and *Oct-Tet-Oct* pathway? Are there any connection among lithium occupation pattern, anion charge, and lattice volume? Therefore, in this work, we made efforts to further understand the roles of anion charge as well as lattice volume on lithium ion occupation and lithium ion migration, and proposed new design principles for developing and optimizing superionic conductors.

RESULTS AND DISCUSSION

The topologies of the close-packed anions of the common lithium ionic conductor materials can be approximately classified into the *fcc*, body-centered cubic (*bcc*), and hexagonal close-packed (*hcp*) sublattices[8]. The anion sublattices of $LiCoO_2$, Li_2MnO_3, $Li_4Ti_5O_{12}$, Li_2S, $LiTiS_2$, and Li_3YBr_6[20] can be exactly matched to *fcc* types. For $Li_7P_3S_{11}$ and $Li_{10}GeP_2S_{12}$, S anion sublattice can be roughly mapped to the *bcc* lattices with some distortions. In both γ-Li_3PS_4 and Li_4GeS_4, S anion sublattices can be closely matched to the *hcp* arrays[8]. In the aforementioned lithium compounds as well as more than half lithium compounds in the Materials Project (MP) database, lithium ions mainly occupy the tetrahedral or octahedral sites, forming the stable tetrahedral or octahedral lithium-anion polyhedra, as shown in the distribution of lithium coordination environments (Supplementary Fig. 1). We find that there are pairs of the adjacent anion tetrahedron and octahedron sharing a triangular face in the *fcc*, *bcc*, and *hcp* anion sublattices. Lithium ion migration between two adjacent *Tet* and *Oct* sites can be regarded as the half migration path for the *Tet-Oct-Tet* or *Oct-Tet-Oct* hopping. Considering *fcc* anion sublattice is much more common than *bcc* and *hcp* anion arrangements (Supplementary Fig. 2), in this work, by DFT calculations, we mainly focused on the ordered *fcc* anion sublattice to efficiently investigate the lithium occupation patterns as well as the lithium ion migration between two adjacent *Oct* and *Tet* sites (two face-sharing octahedron and tetrahedron) from a new perspective of the effect of anion charge as well as lattice volume, from which the new design principles for efficiently searching and optimizing superionic conductors were proposed. The anion charge and lattice volume dependent lithium occupation pattern and lithium ion migration in *bcc*- and *hcp*-type anion sublattices will be further studied in another work.

Anion charge and lattice volume dependent lithium occupation and migration

First, we have calculated the anion Bader charges and lattice volumes of some stable lithium oxides and sulfides from the MP database, to determine the reasonable value ranges of anion charge and lattice volume, as listed in Tables 1 and 2 in Supplementary Information. Figure 1 shows the scatter distributions of anion charge and lattice volume of some lithium oxides and sulfides, and the fitted straight lines approximately demonstrate a positive correlation between anion charge and lattice volume. For the convenience of making good comparison, lattice volumes are averaged to each anion from the volumes of unit cell.

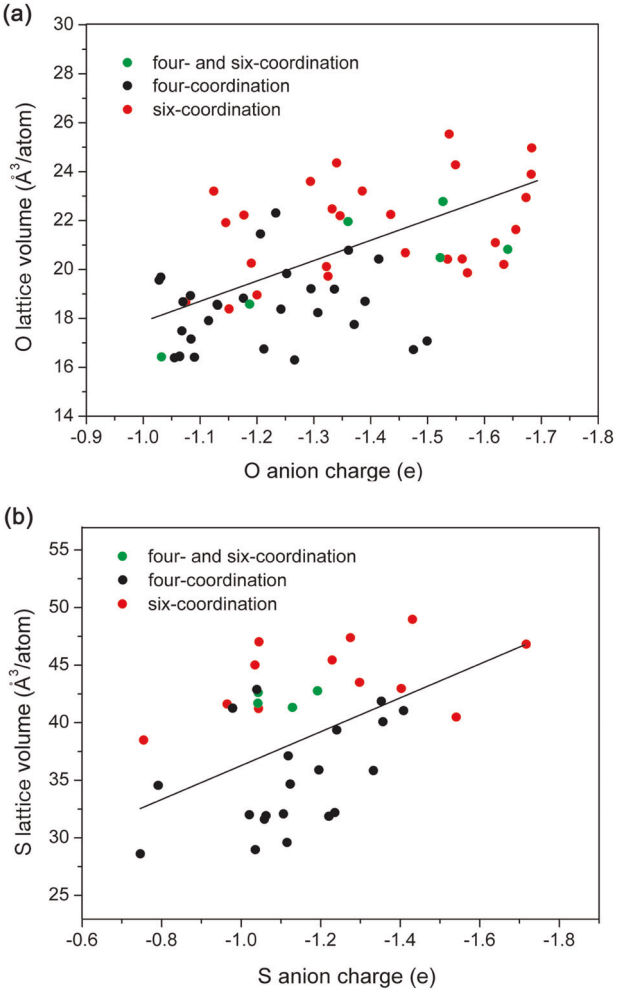

Fig. 1 Value distributions of anion charge and lattice volume. The scatter distributions of anion charges and lattice volumes around the fitted straight lines for some common lithium **a** oxides and **b** sulfides listed in Supplementary Table 1 and 2. Anion charges are calculated by the Bader charge analysis, and lattice volumes are averaged to each anion from the volumes of unit cell.

Then, an artificial *fcc*-type anion sublattice with 48 anions and one single lithium ion (Supplementary Fig. 3) was built to simulate lithium ion migration between two adjacent *Oct* and *Tet* central sites, as the local structure shown in Fig. 2. This computational strategy can allow us directly capture the effect of anion charge and lattice volume, which has been successfully used by Ceder et al.[8]. Then, the nudged elastic band (NEB) calculations were performed to monitor the energy variations for lithium ion migration from an *Oct* site to its adjacent *Tet* site with respect to different anion charges and lattice volumes. Here, different kinds of anion were considered, including O, S, F, Cl, Br, and I anions, and the calculated results of lithium ion migration barriers (E_m) and the energy differences ($E_{tet\text{-}oct}$) between *Tet* Li site and *Oct* Li site are shown as the heat maps in Figs. 3, S4 and S5. Anion charge and lattice volume have significant impacts on E_m and $E_{tet\text{-}oct}$ values for both chalcogen (Fig. 3) and halogen (Supplementary Figs. 4 and 5) anion sublattice systems. In addition, a consistent mechanisms of anion charge and lattice volume on E_m and $E_{tet\text{-}oct}$ are observed for different anion systems. The variation trends of E_m and $E_{tet\text{-}oct}$ with respect to different anion charges and lattice volumes are much more interesting than the absolute values of E_m. Taking O

anion sublattice as an example (Fig. 3a), within different O lattice volume regions, O anion charges have different effects on E_m values for lithium ion migration. However, for a specific O lattice volume, the more negative O anion charges consistently reduce $E_{tet\text{-}oct}$ values (Fig. 3c), and stabilizing LiO_4 tetrahedron. Here, the more negative charges are relative to those charges closed to zero. For example, −1.7*e* is a more negative charge than −0.5*e*. At a constant O anion charge, $E_{tet\text{-}oct}$ values vary from positive to negative, and the relative stabilities of LiO_4 tetrahedron gradually increase when O lattice volumes get larger. In addition, S, F, Cl, Br, and I anion sublattices show the similar effects of anion charge and lattice volume on lithium ion migration and the relative stabilities of lithium-anion tetrahedron. In summary, both the more negative anion charges and large lattice volumes make lithium ions prefer to occupy *Tet* sites.

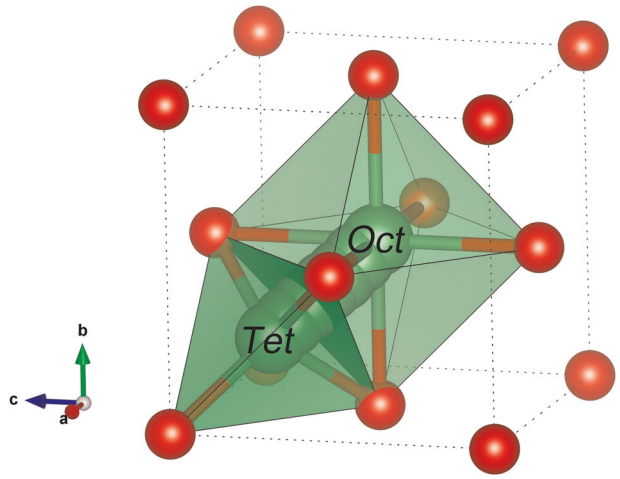

Fig. 2 Local structure of lithium ion migration in *fcc* anion sublattice. Lithium ion migration between two adjacent *Oct* and *Tet* sites in *fcc*-type anion sublattice, which is the local structure from anion sublattice in Supplementary Fig. 3. Lithium ions and anions are colored red and green, respectively.

For the conveniences of clear insights into the effects of anion charge, we chose three representative lattice volumes of O anion systems from heat maps in Fig. 3, and O anion charge dependent energy variations of lithium ion migration between two adjacent *Oct* and *Tet* central sites and the corresponding E_m at three fixed lattice volumes are shown in Fig. 4. When O lattice volume is small, e.g. with a value of ~16.26 Å^3/atom (16.41 Å^3/atom for $R\bar{3}m$-$LiCoO_2$, Supplementary Table 1), the relative energies of LiO_4 are all higher than those of LiO_6 ($E_{tet\text{-}oct} > 0$, Fig. 4a), indicating lithium ions are most stable in *Oct* sites, which are consistent with the fact that lithium oxides with smaller O lattice volumes (16–18 Å^3/atom) show the octahedral lithium occupations (Supplementary Table 1 and Fig. 1a). In addition, the more negative O anion charges would lower the relative energies of LiO_4, and hence reduce the corresponding E_m for lithium ion migration in these O anion

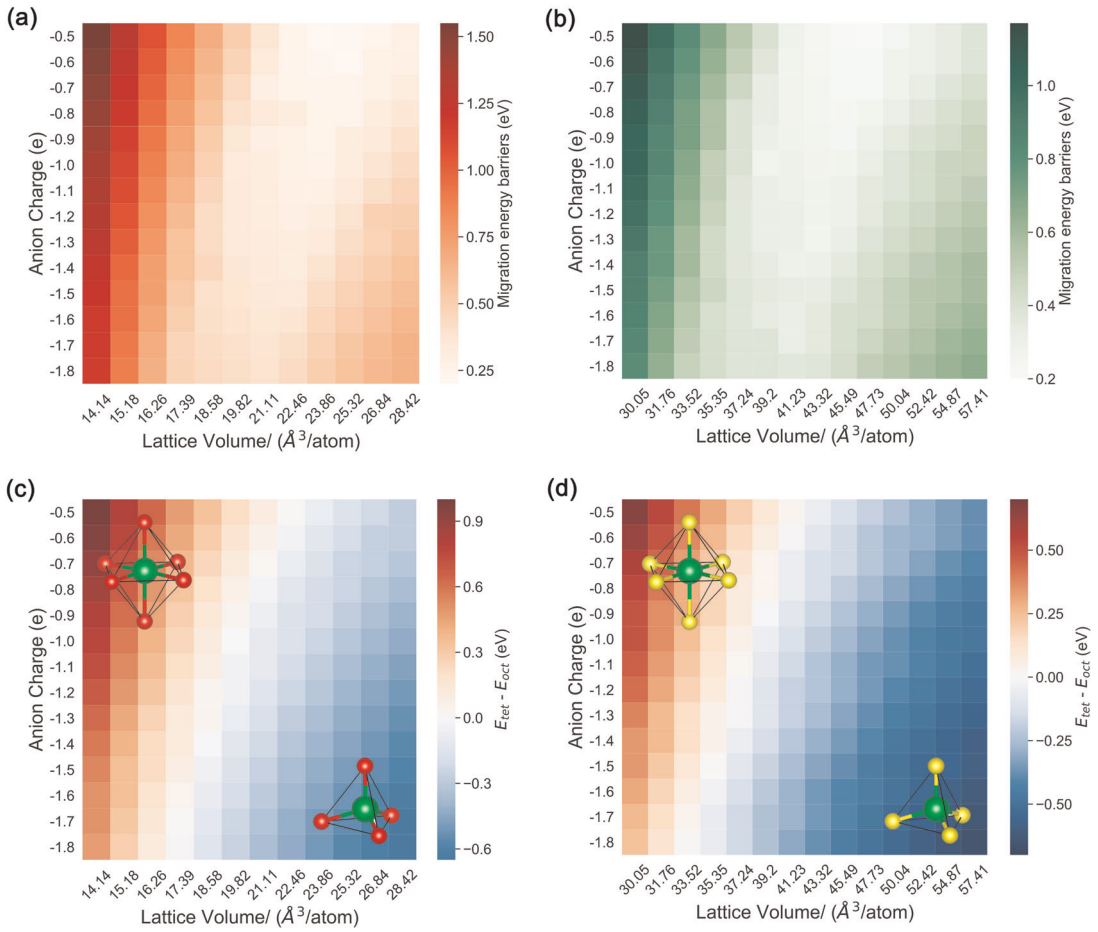

Fig. 3 Anion charge and lattice volume dependent E_m and $E_{tet\text{-}oct}$. Heat maps of the calculated E_m of lithium ion migration between two adjacent *Oct* and *Tet* central sites in the artificial *fcc*-type **a** oxygen and **b** sulfur anion sublattices, and energy differences ($E_{tet\text{-}oct}$) between *Tet* Li site and *Oct* Li site in *fcc*-type **c** oxygen and **d** sulfur anion sublattices with respect to different anion charges and lattice volumes, respectively.

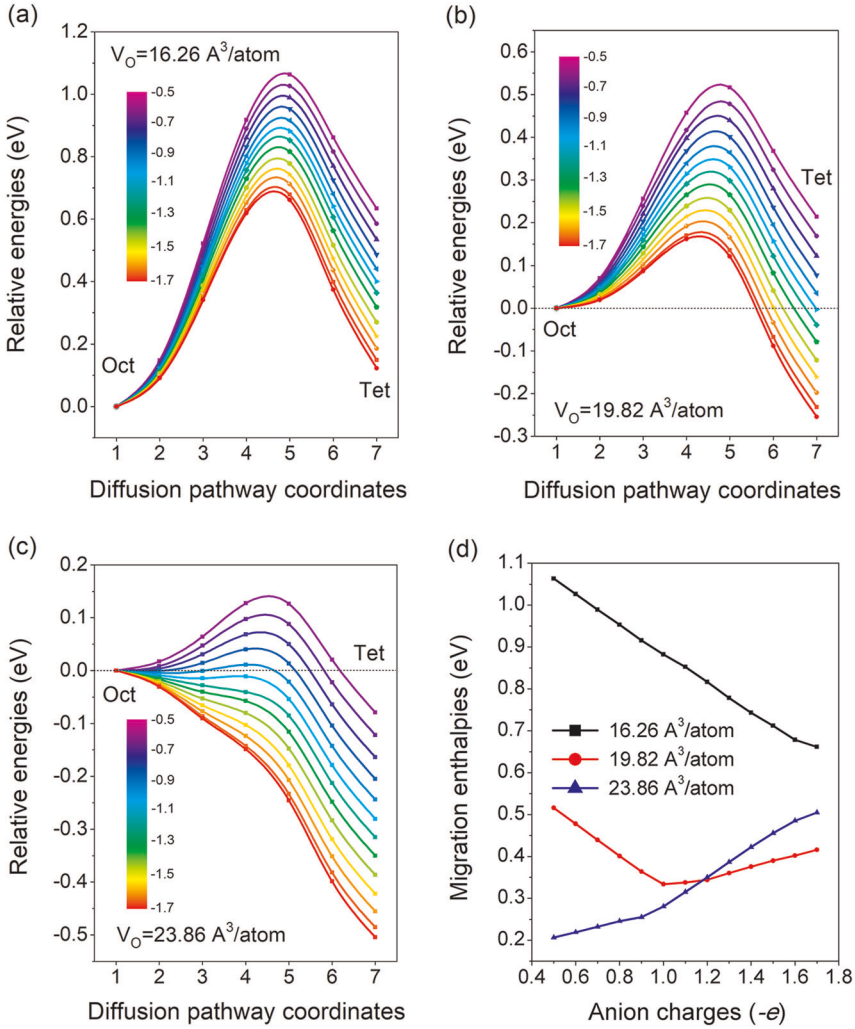

Fig. 4 Energy variations of lithium migration in anion sublattice. DFT calculation monitored energy variations of lithium ion migration between two adjacent *Oct* and *Tet* central sites in *fcc*-type oxygen anion sublattices with respect to different oxygen anion charges and a constant lattice volume of **a** $V_o = 16.26$ Å^3/atom, **b** $V_o = 19.82$ Å^3/atom, **c** $V_o = 23.86$ Å^3/atom, respectively; and **d** E_m of lithium ion migration in *fcc* oxygen anion sublattices.

sublattices with smaller O lattice volumes (Fig. 4d). For O anion systems with medium lattice volumes, e.g. ~19.82 Å^3/atom (19.86, 20,42, and 20.43 Å^3/atom for Li_2SiO_3, Li_2FeSiO_4, and Li_2MnSiO_4, respectively, Supplementary Table 1), with negative O anion charges increasing from −0.5 to −1.7*e*, E_m values would first decrease and then increase (Fig. 4d). This is because the relative energies of LiO_4 are higher than those of LiO_6 ($E_{tet\text{-}oct} > 0$, Fig. 4b) for the systems with the smaller negative O anion charges ($q_O < -1.0$). While more negative O anion charges ($q_O > -1.0$) make the relative energies of LiO_4 lower than those of LiO_6 ($E_{tet\text{-}oct} < 0$) and *Oct* sites no longer stable. At a larger lattice volume, e.g. ~23.86 Å^3/atom (23.67 and 24.97 Å^3/atom for Li_5AlO_4 and Li_2O, respectively, Supplementary Table 1), the relative energies of LiO_4 are lower than those of LiO_6 ($E_{tet\text{-}oct} < 0$, Fig. 4c), indicating lithium ions prefer *Tet* sites at large lattice volumes, as Supplementary Table 1 and Fig. 1a show that lithium oxides with larger O lattice volumes (>21 Å^3/atom) showing tetrahedral lithium occupations. Moreover, we found that lithium ion migrations in these O anion sublattices with large O lattice volumes (~23.86 Å^3/atom) become less sensitive to the increase of negative O anion charges (Fig. 4d). Viewed from Fig. 4d that only when negative O anion charges are <−1.2*e*, the increased O lattice volumes would reduce E_m for lithium ion migration. While the increased O lattice volumes make E_m first decrease and then increase as negative O anion charges are more than −1.2*e*, which is consistent with the earlier study on *fcc* S^{2-} sublattice by Ceder et al.[8]. In summary, the large negative anion charges would deliver high E_m for the tetrahedral lithium ion migration along *Tet-Oct-Tet* pathways, but make lower E_m for the octahedral lithium ion migration along *Oct-Tet-Oct* pathways.

Model validation

The activation energy barrier and jump distance for lithium ion migration are determined by the total energy landscape of lithium. The total energy landscape of lithium ion in an ionic solid can be described by the Coulomb–Buckingham potential model, which can be further divided into the short-ranged Li-anion Pauli repulsive interaction, the short-ranged Li-anion electrostatic attractive interaction, and the longer-ranged Li-cation electrostatic repulsive interaction. The short-ranged Li-anion interactions (Pauli repulsive and electrostatic attractive interaction) are modulated by the high-frequency alternations of the stable lithium occupation sites separated by the activation energy barriers that lithium needs to overcome when squeezing through a small bottleneck to reach the adjacent stable site[10]. While the Li-cation repulsive interactions show much longer modulations on the order of the distance between two cations[10]. The resulting total energy landscapes are mainly set by the Li-anion interactions, so lithium

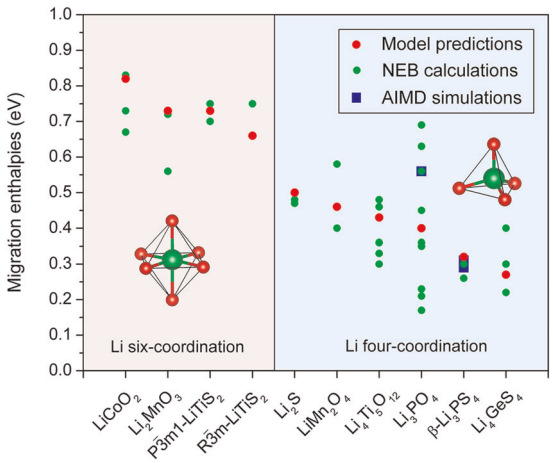

Fig. 5 *fcc* anion sublattice model validation by available data. Comparisons among the predicted E_m from *fcc* anion sublattice model, and NEB calculated E_m for lithium ion migration by *Tet-Oct-Tet* or *Oct-Tet-Oct* pathways, and E_m from AIMD simulations for some lithium compounds with *fcc* anion sublattices. The corresponding E_m data in this figure are also listed in Supplementary Table 3.

ion migration in an ionic compound can be approximatively reduced to lithium ion migration in an anion sublattice model. It is also noted that the Li-cation repulsive interactions also contribute to the total energy landscape to some extents, and the weight of the Li-cation interaction in setting the total energy landscape is set by the arrangements and valance states of cation.

Combining the anion sublattice model (heat maps in Fig. 3) with the calculated Bader charges and lattice volumes (listed in Supplementary Tables 1 and 2) of some lithium oxides and sulfides, the corresponding E_m were predicted, as shown in Fig. 5 and Supplementary Table 3, in comparison with some available NEB and *ab* initio molecular dynamics (AIMD) calculated E_m of lithium compounds with *fcc* anion sublattices. It is found that there are some discrepancies between the predicted E_m and NEB calculated results for some lithium compounds. These deviations may come from the non-negligible Li-cation interactions, distorted anion sublattices, and anisotropic anion polarization of some realistic lithium compounds resulting in different total energy landscapes than those set by our orderly anion sublattice model. It is worth noting that most of these NEB calculated E_m are path and migration mechanism dependent, which are not considered in our anion sublattice model. In addition, even for $LiCoO_2$, $LiMn_2O_4$, and $LiTiS_2$ with only a specific lithium ion migration path, we find that different researchers get quite different NEB results (Supplementary Table 3). Therefore, making comparison between our model predicted E_m and the NEB calculated E_m for a specific path is not meaningful. While E_m from AIMD simulations can be regarded as the statistical average for lithium ion migration along different paths, and validating our model predicted results of lithium compounds by using the corresponding AIMD simulation calculated E_m are meaningful. Unfortunately, the AIMD calculated results for lithium compounds are very rare, and only solid-state electrolytes of γ-Li_3PO_4 and β-Li_3PS_3 are available. It is delightful that our anion sublattice model predicted E_m of 0.32 eV for β-Li_3PS_3 agrees well with the corresponding AIMD calculated results of 0.29 and 0.31 eV. On the other hand, the predicted E_m of 0.50 eV for Li_2S is much close to the NEB calculated results of 0.47 and 0.48 eV[8,21], indicating that lithium ion migration in Li_2S is mainly dominated by the short-ranged interactions between Li cation and its neighboring S anions, and the long-ranged electrostatic repulsion interactions of Li^+–Li^+ in Li_2S do not affect lithium ion migration too much. The long-ranged Li^+–Li^+ repulsion interactions in Li_2S are much smaller than those of Li-cation (Li^+–M, $M = Mn^{3+}$, Si^{4+} or P^{5+}) in the ternary and quaternary lithium compounds, e.g. $LiFePO_4$ and Li_2MnSiO_4. The good accuracy of the predicted E_m for Li_2S firmly validates our anion sublattice model again. Additionally, it can be seen from Fig. 5 that E_m from both model prediction and NEB calculations of lithium four-coordinated compounds are relatively smaller than those of lithium six-coordinated compounds, as least for the above-mentioned oxides and sulfides, which is consistent with the fact of most superionic conductors showing lithium tetrahedral occupations, such as Li_3PO_4, Li_3PS_4, $Li_7P_3S_{11}$, and $Li_{10}GeP_2S_{12}$. Most importantly, beyond the compounds in Supplementary Table 3, E_m of lithium ion migration in other lithium compounds with face-sharing tetrahedron and octahedron can be predicted by our anion sublattice model without DFT calculations, associated with known anion charges and lattice volumes.

To confirm the anion charge-lattice volume maps in Fig. 3, we also have performed AIMD simulations for *fcc*-type sulfur anion sublattice with a single lithium ion. Four models with the maximum and minimum anion charge-lattice volume were considered, i.e. −0.5 *e* & 31.76 Å^3/atom, −0.5*e* & 54.87 Å^3/atom, −1.7*e* & 31.76 Å^3/atom, and −1.7*e* & 54.87 Å^3/atom. The 500 K AIMD videos (.mp4 files in Supplementary Videos) clearly show that lithium steadily vibrates around the center of *Oct* site in the system with small lattice volume of 31.76 Å^3/atom regardless of different anion charges, while lithium spontaneously transfers from the instable *Oct* site to the stable *Tet* site in the large sulfur anion system with a lattice volume of 54.87 Å^3/atom, which are fully consistent with the picture of energy differences ($E_{tet\text{-}oct}$) between *Tet* and *Oct* Li site (Fig. 3d). Moreover, it is found from AIMD movies that large anion charge of −1.7*e* make preferable diffusivity (greater vibration amplitude) of the octahedrally occupied lithium in the small sulfur anion lattice of 31.76 Å^3/atom, while the small anion charge of −0.5*e* make superior diffusivity of the tetrahedrally occupied lithium in the large sulfur anion lattice of 54.87 Å^3/atom, which are in good accordance with the E_m map in Fig. 3b.

The anion charge dependent E_m for lithium ion migration along *Tet-Oct-Tet* and *Oct-Tet-Oct* pathways are also confirmed by some reported lithium compounds. Our previous work on the chalcopyrite-structured $LiMS_2$ (M are transition metals, from Ti to Ni) materials with tetrahedral lithium occupations shows that the smaller negative S anion charges resulted from the smaller electronegativity difference between transition metal and sulfur element would lead to lower E_m for lithium ion migration along *Tet-Oct-Tet* pathways[15]. Mo et al. found E_m for the tetrahedral lithium ion migration along *Tet-Oct-Tet* pathways in a *fcc* monovalent S^- anion sublattice is much lower that of the bivalent S^{2-} anion sublattice with the same lattice volumes[16]. For the spinel structured $LiAlCl_4$, Li_2MgCl_4, and Li_2MgBr_4 with tetrahedral lithium occupations, the very active Mg and Al elements enable more negative anion charges, eventually showing higher E_m for the *Tet-Oct-Tet* lithium ion migration. Similar effect can be also found in $Li_{10}MP_2S_{12}$ (M = Ge and Sn) materials with tetrahedral lithium occupations. The higher electronegativity of Ge *vs*. Sn (2.0 *vs* 1.7[22]) give rise to less electron densities on S anions in $Li_{10}GeP_2S_{12}$, leading to the smaller negative anion charges, and thereby show relatively lower E_m compared to $Li_{10}SnP_2S_{12}$[17]. The above reported lithium compounds with tetrahedral lithium occupations consistently obey the rule of the smaller negative anion charges leading to higher E_m for the tetrahedral lithium ion migration, proposed in the foregoing model analyses of Fig. 4c. On the other hand, our previous research on lithium iodides[19], Li_3MI_6 (M = Sc, Y, and La) with octahedral lithium occupations, shows that the largest I anion negative charges of Li_3LaI_6 resulted from the most active La (Pauling electronegativity χ_A, Sc (χ_A = 1.36) > Y (χ_A = 1.22) > La (χ_A = 1.10)[23,24]) lead to the lowest phonon DOS center of lithium and smallest E_m for lithium ion

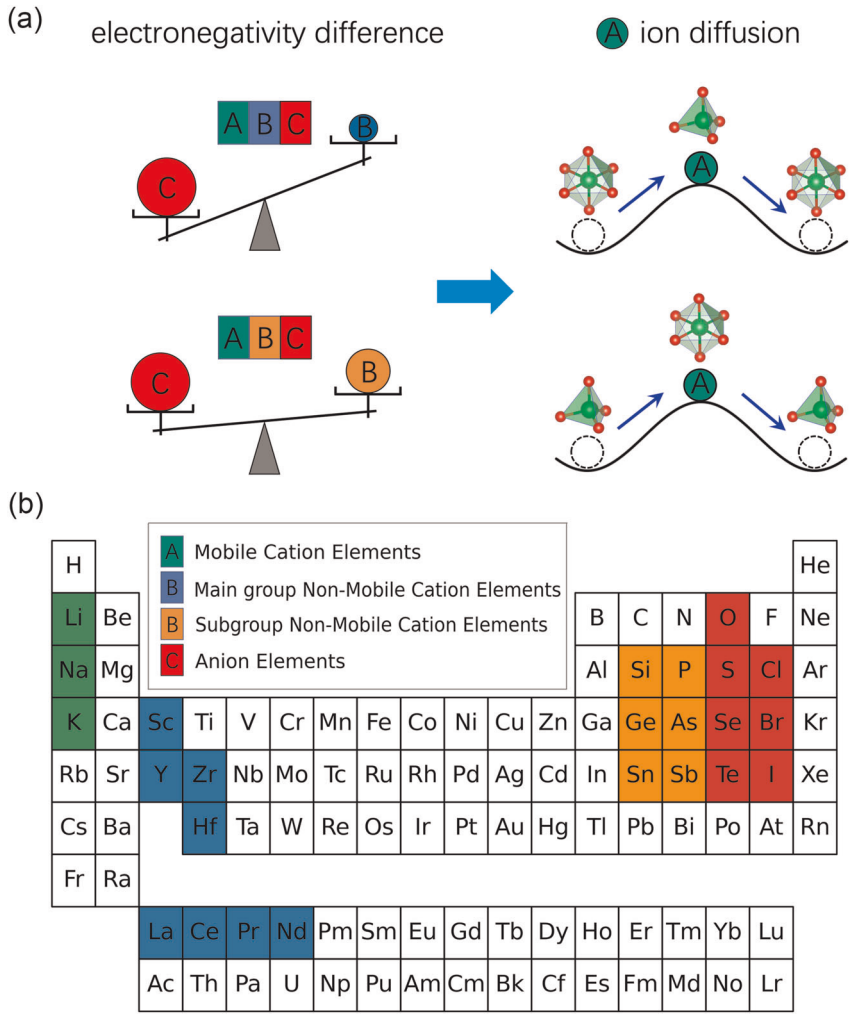

Fig. 6 Design principles for fast A ion migration in the ABC ternary compounds. a Schematic diagrams of the effects of the electronegativity differences between non-mobile cation elements B and anion elements C on A ion migration, **b** the recommended choices of the non-mobile cation element B in the periodic table of element for achieving fast A ion migration.

migration along *Oct-Tet-Oct* pathways, which are also in good agreement with the foregoing model analyses of Fig. 4a. We also find E_m change of lithium ion migration along *Oct-Tet-Oct* pathways in the gradually charged Li_xCoO_2[25,26], $P\bar{3}m1$-Li_xTiS_2[27] and $P6_3/mmc$ -Na_xCoO_2[28] cathodes match our anion charge-lattice volume map, that is with more Li or Na extraction from these layered structures, the lattice parameter *c* as well as the anion charge would decrease to some extents[27,29], making the values of anion charge-lattice volume locate at the more top left portion in the anion charge-lattice volume heat maps (Fig. 4) and eventually increasing E_m. In sum, the anion charge-lattice volume maps (change trends of E_m with respect to anion charge and lattice volume) of anion sublattice model are reasonable and creditable, although the predicted absolute values of E_m from anion sublattice model are different from the NEB data especially for those compounds with high Li-cation repulsive interactions or large anion sublattice distortions.

New principles for developing superionic conductors with *fcc* anion sublattices

In ternary, quaternary and even more polynary alkali metal compounds, anion charges are usually affected by the electronegativity of the non-alkali metal elements, as confirmed by some previous work[15,17]. The atomic radius and valence electron configuration of the non-alkali metal element determines its coordination environment and crystal volume, eventually affecting the corresponding lattice volumes. The above anion sublattice model analyses clearly show that anion charge and lattice volume significantly affect alkali metal ion occupation and ion migration. It is expected to achieve low E_m for alkali metal ion migration by adjusting the non-alkali metal element without changing the crystal structure. It is also worth noting that the largely distorted anion sublattice would cause the distorted lithium occupations and Li-anion polyhedra, increasing the instability of lithium and eventually leading to the more frustrated energy landscape for fast lithium ion diffusion[10].

Here, based on the above findings, general principles for developing and optimizing new ternary ABC type lithium, sodium or even multivalent metal superionic conductors with *fcc* anion sublattices are summarized: (i) for the superionic conductors with stable A ion octahedral occupation sites, the large electronegativity difference between anion element C and non-mobile cation element B is essential for achieving excellently fast A ion migration, as shown in Fig. 6a, and the applicable non-mobile cation element B should give preference to the elements located at the left bottom of the periodic table with small electronegativity, as shown in Fig. 6b. The chemical components of the very

recently reported halide-type lithium superionic conductors with relatively high lithium ionic conductivities of ~1 mS/cm at room temperature, e.g. Li_3YBr_6[20], and Li_3ErI_6[30], are completely in conformity with our octahedron principle; (ii) for the superionic conductor with stable A ion tetrahedral occupation sites, the small electronegativity difference between anion element C and non-mobile cation element B is essential for achieving excellently fast A ion migration, as shown in Fig. 6a, and the applicable non-mobile cation element B should give preference to the elements located at the right top of the periodic table of elements with large electronegativity, which are close to but less than that of C element, as shown in Fig. 6b. The chemical components of the most superionic conductors with lithium tetrahedral occupations, such as Li_3PS_4[31,32], $Li_7P_3S_{11}$[33], $Li_{1+2x}Zn_{1-x}PS_4$[9], and Li_2CuPS_4[18] with *Tet-Oct-Tet* lithium migration pathways, perfectly fit with this tetrahedron principle. We hope that these two guiding principles will contribute to the design and optimization of superionic conductors.

In summary, the *fcc* anion sublattice model show that anion charge and lattice volume significantly affect lithium ion occupation and ion migration, which is confirmed by many reported materials. Both the more negative anion charges and large lattice volumes would enhance the relative stabilities of tetrahedral lithium occupations. There are opposite effects of anion charge on activation energy barrier for lithium ion migration along *Tet-Oct-Tet* and *Oct-Tet-Oct* pathways in the *fcc*-type anion sublattices. For tetrahedral lithium ion migration along *Tet-Oct-Tet* pathways through an *Oct* transition state, the smaller negative anion charge is, the lower the lithium ion migration barrier is. While for octahedral lithium ion migration along *Oct-Tet-Oct* pathways through a *Tet* transition state, the more negative anion charge is, the lower the lithium ion migration barrier is. Most importantly, new design principles for developing and optimizing advanced superionic conductors with *fcc* anion sublattices were proposed based on the full understandings of anion sublattice model. Low E_m for ion migration would be achieved by adjusting the non-mobile cation element within the same crystal structure to obtain the desired electronegativity differences between the anion element and non-mobile cation element.

METHODS

This work is based on the density functional theory (DFT) calculations performed by using the Vienna ab initio Simulation Package (VASP) software. The interaction between ion cores and valence electrons described by the projector augmented wave (PAW) method[34]. The generalized gradient approximation (GGA)[35] in the form of Perdew–Burke–Ernzerhof (PBE) exchange functional[36] was used to solve the quantum states of electron. The plane-wave energy cutoff is set to 500 eV. The Monkhorst–Pack method[37] with $1 \times 1 \times 2$ *k*-point mesh is employed for the Brillouin zone sampling of the super lattice. The convergence criteria of energy and force are set to 10^{-5} eV/atom and 0.01 eV/Å, respectively. The anion charges of lithium compounds were calculated by using the Atoms in Molecules method (Bader charge analysis)[38]. The energy variations and migration barriers of lithium ion migration in *fcc*-type anion sublattices with 48 anions (Supplementary Fig. 3) are calculated by the nudged elastic band (NEB) method[39,40]. The anion charges are changed by the uniform background charge of the sublattice system. Only the one migrating lithium ion is allowed to relax, while the other anions are fixed in their initial positions, and this method can be also found in Ceder's work[8].

DATA AVAILABILITY

The data generated or analyzed for this work are openly available at the website of https://github.com/zhenming-xu/Data-and-Codes-for-Anion-charge-lattice-volume-dependent-Li-ion-migration.

CODE AVAILABILITY

The codes of get the distribution of anion sublattice type and lithium coordination environment of lithium compounds from the Materials Project Database are publicly available at GitHub website, https://github.com/zhenming-xu/Matching-anion-framework-and-Li-local-environments-from-MP-database.

Received: 27 November 2019; Accepted: 10 April 2020;
Published online: 07 May 2020

REFERENCES

1. Zhang, Z. et al. New horizons for inorganic solid state ion conductors. *Energy Environ. Sci.* **8**, 1945–1976 (2018).
2. Judez, X., Eshetu, G. G., Li, C., Rodriguez-Martinez, L. M., Zhang, H. & Armand, M. Opportunities for rechargeable solid-state batteries based on Li-intercalation cathodes. *Joule* **2**, 2208–2224 (2018).
3. Sun, C., Liu, J., Gong, Y., Wilkinson, D. P. & Zhang, J. Recent advances in all-solid-state rechargeable lithium batteries. *Nano Energy* **33**, 363–386 (2017).
4. Murugan, R., Thangadurai, V. & Weppner, W. Fast lithium ion conduction in garnet-type $Li_7La_3Zr_2O_{12}$. *Angew. Chem. Int. Ed.* **46**, 7778–7781 (2007).
5. Morimoto, H. et al. Preparation of lithium ion conducting solid electrolyte of NASICON-type $Li_{1+x}Al_xTi_{2-x}(PO_4)_3$ ($x = 0.3$) obtained by using the mechanochemical method and its application as surface modification materials of $LiCoO_2$ cathode for lithium cell. *J. Power Sources* **240**, 636–643 (2013).
6. Kamaya, N. et al. A lithium superionic conductor. *Nat. Mater.* **10**, 682–686 (2011).
7. Seino, Y., Ota, T., Takada, K., Hayashi, A. & Tatsumisago, M. A sulphide lithium super ion conductor is superior to liquid ion conductors for use in rechargeable batteries. *Energy Environ. Sci.* **7**, 627–631 (2014).
8. Wang, Y. et al. Design principles for solid-state lithium superionic conductors. *Nat. Mater.* **14**, 1026–1031 (2015).
9. Richards, W. D., Wang, Y., Miara, L. J., Kim, J. C. & Ceder, G. Design of $Li_{1+2x}Zn_{1-x}PS_4$, a new lithium ion conductor. *Energy Environ. Sci.* **9**, 3272–3278 (2016).
10. Di Stefano, D. et al. Superionic diffusion through frustrated energy landscape. *Chem* **5**, 1–11 (2019).
11. Rong, Z. et al. Materials design rules for multivalent ion mobility in intercalation structures. *Chem. Mater.* **27**, 6016–6021 (2015).
12. He, X., Zhu, Y. & Mo, Y. Origin of fast ion diffusion in super-ionic conductors. *Nat. Commun.* **8**, 15893 (2017).
13. Xiao, R., Li, H. & Chen, L. High-throughput design and optimization of fast lithium ion conductors by the combination of bond-valence method and density functional theory. *Nat. Commun.* **5**, 14227 (2015).
14. Xu, B. & Meng, S. Factors affecting Li mobility in spinel $LiMn_2O_4$-a first-principles study by GGA and GGA+U methods. *J. Power Sources* **195**, 4971–4976 (2010).
15. Xu, Z. M., Bo, S. H. & Zhu, H. $LiCrS_2$ and $LiMnS_2$ cathodes with extraordinary mixed electron-ion conductivities and favorable interfacial compatibilities with sulfide electrolyte. *ACS Appl. Mater. Interfaces* **10**, 36941–36953 (2018).
16. Wang, S. et al. Lithium chlorides and bromides as promising solid-state chemistries for fast ion conductors with good electrochemical stability. *Angew. Chem. Int. Ed.* **58**, 8039–8043 (2019).
17. Krauskopf, T., Culver, S. P. & Zeier, W. G. Bottleneck of diffusion and inductive effects in $Li_{10}Ge_{1-x}Sn_xP_2S_{12}$. *Chem. Mater.* **30**, 1791–1798 (2018).
18. Xu, Z., Chen, R. & Zhu, H. A Li_2CuPS_4 superionic conductor: a new sulfide-based solid-state electrolyte. *J. Mater. Chem. A* **7**, 12645–12653 (2019).
19. Xu, Z. et al. Influence of anion charge on Li ion diffusion in a new solid-state electrolyte, Li_3LaI_6. *Chem. Mater.* **31**, 7425–7433 (2019).
20. Asano, T. et al. Solid halide electrolytes with high lithium-ion conductivity for application in 4 V class bulk-type all-solid-state batteries. *Adv. Mater.* **30**, 1803075 (2018).
21. Moradabadi, A. & Kaghazchi, P. Thermodynamics and kinetics of defects in Li_2S. *Appl. Phys. Lett.* **108**, 213906 (2016).
22. Martienssen, W. & Warlimont, H. *Springer Handbook Of Condensed Matter And Materials Data* (Springer Science & Business Media, New York, 2006).
23. Allred, A. L. Electronegativity values from thermochemical data. *J. Inorg. Nucl. Chem.* **17**, 215–221 (1961).
24. Pauling, L. *The Nature Of The Chemical Bond And The Structure Of Molecules And Crystals: An Introduction To Modern Structural Chemistry* (Cornell University Press, New York, 1960).
25. Okubo, M., Tanaka, Y., Zhou, H., Kudo, T. & Honma, I. Determination of activation energy for Li ion diffusion in electrodes. *J. Phys. Chem. B* **113**, 2840–2847 (2009).
26. Van der Ven, A. Lithium diffusion in layered Li_xCoO_2. *Electrochem. Solid State Lett.* **3**, 301 (1999).
27. Van der Ven, A., Thomas, J. C., Xu, Q., Swoboda, B. & Morgan, D. Nondilute diffusion from first principles: Li diffusion in Li_xTiS_2. *Phys. Rev. B* **78**, 104306 (2008).

28. Mo, Y., Ong, S. P. & Ceder, G. Insights into diffusion mechanisms in P2 layered oxide materials by first-principles calculations. *Chem. Mater.* **26**, 5208–5214 (2014).
29. Takahashi, Y. et al. Structure and electron density analysis of electrochemically and chemically delithiated $LiCoO_2$ single crystals. *J. Solid State Chem.* **180**, 313–321 (2007).
30. Schlem, R., Bernges, T., Li, C., Kraft, M., Minafra, N. & Wolfgang, Z. A lattice dynamical approach for finding the lithium superionic conductor Li_3ErI_6. *ACS Appl. Energy Mater.* https://doi.org/10.1021/acsaem.0c00147 (2020).
31. Tachez, M., Malugani, J.-P., Mercier, R. & Robert, G. Ionic conductivity of and phase transition in lithium thiophosphate Li_3PS_4. *Solid State Ion.* **14**, 181–185 (1984).
32. Homma, K. et al. Crystal structure and phase transitions of the lithium ionic conductor Li_3PS_4. *Solid State Ion.* **182**, 53–58 (2011).
33. Yamane, H. et al. Crystal structure of a superionic conductor, $Li_7P_3S_{11}$. *Solid State Ion.* **178**, 1163–1167 (2007).
34. Blöchl, P. E. Projector augmented-wave method. *Phys. Rev. B* **50**, 17953–17979 (1994).
35. Perdew, J. P., Burke, K. & Ernzerhof, M. Generalized gradient approximation made simple. *Phys. Rev. Lett.* **77**, 3865–3868 (1996).
36. Kohn, W. & Sham, L. J. Self-consistent equations including exchange and correlation effects. *Phys. Rev.* **140**, A1133–A1138 (1965).
37. Monkhorst, H. J. & Pack, J. D. Special points for Brillouin-zone integrations. *Phys. Rev. B* **13**, 5188–5192 (1976).
38. Yu, M. & Trinkle, D. R. Accurate and efficient algorithm for Bader charge integration. *J. Chem. Phys.* **134**, 064111 (2011).
39. Henkelman, G. & Jónsson, H. Improved tangent estimate in the nudged elastic band method for finding minimum energy paths and saddle points. *J. Chem. Phys.* **113**, 9978–9985 (2000).
40. Shi, S. et al. Multi-scale computation methods: their applications in lithium-ion battery research and development. *Chin. Phys. B* **25**, 018212 (2016).

ACKNOWLEDGEMENTS

This work is supported by the National Natural Science Foundation of China (51602196), Shanghai Automotive Industry Corporation (1714), and Materials Genome Initiative Center at Shanghai Jiao Tong University. Z.X. is much grateful to the support of the China Scholarship Council (CSC, scholarship No. 201906230117). All simulations were performed at the Shanghai Jiao Tong University High Performance Computing Center. We also thank Dr. S.H. Bo for the discussions.

AUTHOR CONTRIBUTIONS

H.Z. designed this research and wrote the paper; Z.X. performed the DFT calculations; X.C. and R.C. analyzed the data; and X.L. revised the paper and made suggestions. All authors discussed and commented on the paper.

COMPETING INTERESTS

The authors declare no competing interests.

ADDITIONAL INFORMATION

Supplementary information is available for this paper at https://doi.org/10.1038/s41524-020-0324-7.

Correspondence and requests for materials should be addressed to H.Z.

Reprints and permission information is available at http://www.nature.com/reprints

Publisher's note Springer Nature remains neutral with regard to jurisdictional claims in published maps and institutional affiliations.